Hindawi
Science and Technology of Nuclear Installations
Volume 2023, Article ID 3337670, 12 pages
https://doi.org/10.1155/2023/3337670

Research Article

Steam-Jet Evaluation for Predicting Leakage Behavior and Interpretation of Experimental Verification

Dae Kyung Choi,[1] **Won Man Park**,[1] **Woo-Shik Kim**,[2] **Dong-Jin Euh**,[2] **Tae-Soon Kwon**,[2] **and Choengryul Choi**[1]

[1]*Elsoltec Inc, Yongin, Republic of Korea*
[2]*Korea Atomic Energy Research Institution, Daejeon, Republic of Korea*

Correspondence should be addressed to Choengryul Choi; crchoi@elsoltec.com

Received 7 October 2022; Revised 2 February 2023; Accepted 21 February 2023; Published 7 March 2023

Academic Editor: Iztok Tiselj

Owing to pipe thinning, fatigue damage, and aging, pipes, valves, and devices installed in the primary and secondary systems of nuclear power plants may leak high-temperature/high-pressure reactor coolant. Thus, a system must be developed to determine if the leakage is exceeding the operating limit of the nuclear power plant, thereby mitigating any loss of life or economic loss in such cases. In this study, a validated numerical analysis method was established to initially simulate the leakage behavior and subsequently to evaluate the small amount of leakage in the compartment. For this purpose, a vapor-jet collision test in the compartment and a vapor-jet test in the pipe were performed; numerical analysis was conducted, and comparative analysis was performed to verify the validity of the established method. The evaluation results suggested that the proposed numerical analysis method could optimally simulate the flow characteristics of the steam jet. Notably, compared to the existing evaluation method, the proposed approach simulated a more detailed behavior of the jet formed at the leakage point. In future research, the results of this study (data) will be used to inform the design of the second phase of the leak-capture system and will be served as the foundation for a performance-optimization study on the capture system.

1. Introduction

The primary and secondary systems of nuclear power plants consist of several pipes, valves, and equipment. Thus, accidents involving leakage of the reactor coolant under conditions of high temperature and pressure may occur owing to thinning of the pipes, fatigue damage due to vibration of equipment, and aging of nuclear power plants [1–3]. In 2008, in the Kori Nuclear Power Plant Unit 3, which was in its normal operational state, a leak occurred at the drain valve weld on the B side of the steam generator. In particular, a leak occurred in the pipeline, and measures were taken to manually stop the reactor [4, 5]. Thus, if a small amount of leakage occurs that exceeds the operational limit of the nuclear power plant, then such a mishap may cause economic loss due to the shutdown of the nuclear power plant or even result in harm and loss of human life due to the leakage of radioactive material.

In the existing pressurized light-water reactor, in accordance with the regulatory guidelines (KINS/RG-N06.01) for detecting a small leak at the level of 1 gpm within 1 hour, the leakage is detected by measuring the radioactivity in the air of the containment building, the humidity change, and water-level change in the water tank. However, recent cases of leakages in nuclear power plants have demonstrated that the small-leakage monitoring performance of the existing reactor-leakage monitoring system is insufficient, and technical improvement is required in the field of small-leak monitoring [6]. Accordingly, a small leak detection system is being actively researched for its development. The Korea Atomic Energy Research Institute has developed an acoustic leak-monitoring system over three years of research, initiated in 2006, and in 2012, they developed a leak-monitoring technology for nuclear power plants

using video signals. Recently, a leak-detection technology has been developed for the real-time monitoring of unidentified leaks in the reactor-coolant system [6].

When a trace amount of leakage occurs in a structure or pipe under high-temperature/high-pressure conditions, the leakage characteristic can be classified as overheated, saturated, and undercooled, and supersonic jets can be formed in the leakage. The supersonic jet flow is formed as an overexpanded flow when the pressure at the nozzle outlet (rupture) is lower than the back pressure, and the pressure at the nozzle outlet increases as the pressure upstream of the nozzle increases. If this pressure is higher than the ambient pressure, an underexpanded jet is formed [7, 8]. When the nozzle pressure ratio (NPR) is small, the shape of the jet is formed as a continuous cell structure. On the contrary, when NPR increases as the nozzle upstream pressure increases, a highly underexpanded jet with complex physics occurs as shown in Figure 1 [8, 9]. The flow discharged from the nozzle rapidly expands owing to the imbalance caused by the high pressure, and an expansion wave is generated. As the generated wave propagates, it encounters the outer boundary of the jet and is reflected, and these waves combine to generate barrel shock. In addition, the Mach disk occurs at a distance of more than several times the nozzle diameter, and the flow after the Mach disk is subsonic. However, a supersonic speed is maintained downstream of the barrel shock. In view of such a complex physical phenomenon occurring in the leakage section, before developing a leakage-detection technology, a numerical analysis technique considering the physical characteristics of the compressible flow should be established to evaluate the leakage behavior.

This study for evaluating the trace leakage in the compartment is segmented into two stages. The first step involves the establishment of a proven methodology of numerical analysis for simulating the leakage behavior, and the second step is a performance evaluation and optimization study of the collection system to collect the leakage through this system. In this study, as the first step in the development of the technology for evaluating a trace amount of leakage in a compartment, a numerical analysis methodology was established to simulate the leakage behavior, and the analysis methodology established for the leak-simulation test was used to validate this methodology. Thereafter, numerical analysis based on computational fluid dynamics (CFD) was performed under the same conditions as those of the experiment. The established analysis methodology was validated through a comparison of simulation results with CFD analysis results and a comparison with the existing evaluation model for the jet range of influence (ZOI).

2. Numerical Analysis Method

2.1. Governing Equations. When a crack forms in the piping or piping joint of the coolant system of the reactor, the coolant leaks through the crack, and a supersonic steam jet may be formed. When the supersonic steam jet is emanated into the surrounding atmosphere, a supersonic underexpanded jet is formed, which is marked by the onset of compressible flow characteristics, such as a barrel shock wave and Mach disk. Essentially, the governing equation for

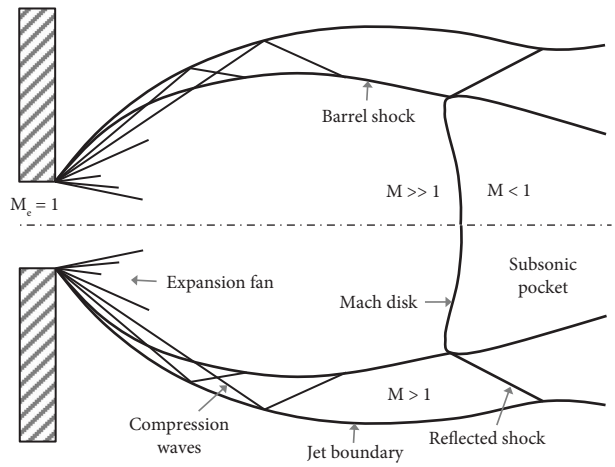

Figure 1: Schematic of a supersonic underexpanded jet.

numerically evaluating this compressive flow comprises a continuity (equation (1)), a momentum (equation (2)), and an energy (equation (3)) as follows:

$$\frac{\partial \rho}{\partial t} + \nabla \bullet (\rho \vec{u}) = 0, \tag{1}$$

$$\frac{\partial}{\partial t}(\rho \vec{u}) + \nabla \bullet (\rho \vec{u}\,\vec{u}) = -\nabla P + \nabla \bullet (\bar{\bar{\tau}}) + \rho \vec{g}, \tag{2}$$

$$\frac{\partial}{\partial t}(\rho E) + \nabla \bullet (\vec{u}(\rho E + P)) = \nabla\left(k_{eff}\nabla T + \left(\bar{\bar{\tau}}_{eff} \bullet \vec{u}\right)\right). \tag{3}$$

In equations (2) and (3), $\bar{\bar{\tau}}$ denotes the stress tensor, which is calculated using equation (4) as follows:

$$\bar{\bar{\tau}} = \mu\left[\left(\nabla \vec{u} + \vec{u}^{T}\right) - \frac{2}{3}\nabla \bullet \vec{u} I\right]. \tag{4}$$

The vapor was assumed to be an ideal gas ($\gamma = 1.3$ [10]), and the total pressure and total temperature for the compressible flow were calculated as follows:

$$\frac{P_0}{P} = \left(1 + \frac{\gamma - 1}{2}M^2\right)^{\gamma/(\gamma-1)},$$

$$\frac{T_0}{T} = 1 + \frac{\gamma - 1}{2}M^2, \tag{5}$$

$$M = \frac{u}{\sqrt{\gamma R T}}.$$

To account the effect of turbulence on supersonic steam jets, the standard k–ε, realizable k–ε, and k–ω shear stress transport (SST) models are widely used because of their excellent convergence and stability among the Reynolds-averaged Navier–Stokes (RANS) equations-based turbulence models. The standard k–ε model tends to slightly overestimate the flow direction characteristics and underestimate the thickness of the flow/temperature boundary layer, and thus, this model is primarily suitable for simulating the strong-level turbulent flow phenomenon. The realizable k–ε model can predict the dissipation rate

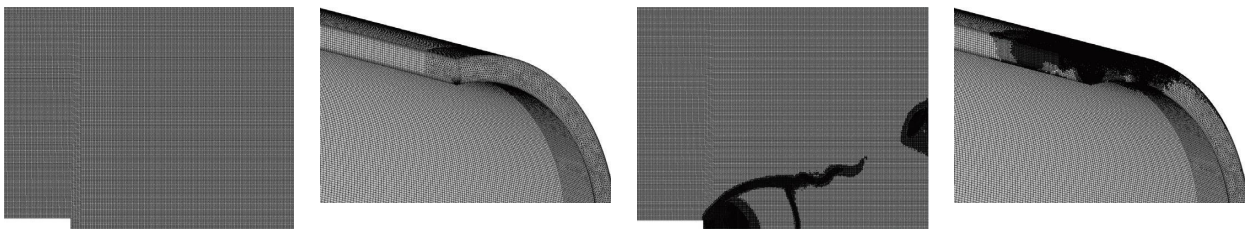

(a) (b) (c) (d)

Figure 2: Grid system with dynamic gradient-based mesh adaptation: (a) initial (2D), (b) initial (3D), (c) final (2D), and (d) final (3D).

distribution of planar and circular jets more accurately than the standard k–ε model via its improved method for calculating the turbulence viscosity. Notably, the boundary-layer properties can be better predicted than the standard k–ε in large pressure gradients, separation, and recirculation flows [11]. Moreover, the k–ω SST model is advantageous as it can be widely used for a relatively wide range of turbulence intensity (Re number); this is because this model selectively leverages the boundary-layer approximation equation according to the flow conditions. In this study, to establish an appropriate methodology for simulating/evaluating the leakage behavior, sensitivity analysis was performed on the aforementioned turbulence model, and an appropriate turbulence model was selected. The sensitivity analysis results are described in Section 4 herein.

2.2. Main Numerical Analysis Techniques. Steady-state compressible flow analysis was performed via ANSYS Fluent v18.0, which is a CFD code based on the finite volume method. A two-dimensional analysis domain was employed in the analysis of the steam-jet collision experiment (Section 3) in the compartment under axisymmetric conditions, and a numerical calculation was performed using a three-dimensional analysis domain in the analysis of the steam-jet leakage experiment (Section 4) in the pipe. Additionally, by using the dynamic gradient-based mesh-adaptation technique, the initial grid (Figures 2(a) and 2(b)) was divided into the region where the pressure gradient was large during the calculation process, and a denser grid (Figures 2(c) and 2(d)) was automatically constructed. Generally, density-based solvers are recommended for compressible flow analysis; however, they can only be applied to single-phase flows. Considering this drawback, in this study, an analysis methodology was established using a pressure-based solver to expand the analysis methodology for two-phase flow in the future. In addition, the coupled algorithm was applied as a pressure-velocity coupling technique. The coupled solver offered excellent numerical stability and yielded a high efficiency for the phenomenon in which the compressible and incompressible flows existed simultaneously [12]. The numerical analysis technique used in this study was verified on the basis of a benchmark study of the Marviken jet impingement test [13] conducted by the Electric Power Research Institute (EPRI; United States) and their verification analysis of the experiments [14].

2.3. Entrance Condition. When a pipe ruptures, the flow rate of steam passing through the rupture possesses a specific critical value depending on the condition of the upstream pipe. In particular, if the back pressure (P_b) decreases, while the upstream pressure (P_0) of the flow passing through the fracture is constant, the flow rate gradually increases, and when the back pressure reaches a certain pressure, the flow rate attains its maximum value, i.e., the flow does not increase further. This state is called critical flow, and the flow rate and back pressure under the critical flow state are called the critical mass flux (G_c) and critical pressure (P_c), respectively [15].

To directly simulate such a critical flow phenomenon in the CFD analysis, the shape and physics inside the fractured pipe must be considered; thus, this consideration may considerably raise the computational resources required for this analysis. Therefore, in this study, the critical flow rate and critical pressure at the pipe breakage were obtained via separate calculations, and these parameters were set as the flow-rate boundary condition and the breakage pressure condition in the CFD analysis.

To obtain the flow rate and pressure of the critical flow passing through the pipe break, a homogeneous equilibrium model (HEM) was utilized. HEM can accurately predict the critical flow rate and throat pressure under high qualities [16]. These models are used in ANSI/ANS-58.2 (1988) by predicting well the critical flow rate of saturated and two-phase jet flow well [10, 17]. In particular, iterative calculation of equation (6) was required for evaluating the critical flow: the critical flow rate (G_c) and critical pressure (P_c) could be obtained by numerically processing the process of determining the point (inflection point) at which the flow rate (G) was maximized, while the P_b decreased under the condition of $P_b/P_0 = 1$. The X (equilibrium thermodynamic quality) can be calculated using equation (7) [18] as follows:

$$G = \frac{2}{v_f(P_b) + X v_{fg}(P_b)} \left(h_0 - h_f(P_b) - X h_{fg}(P_b)\right), \quad (6)$$

$$X = \frac{s_0 - s_f(P_b)}{s_{fg}(P_b)}, \quad (7)$$

where v represents the specific volume, the subscript f denotes the saturated water, subscript fg depicts the difference in state variables of saturated steam and saturated water, and subscript 0 symbolizes the stagnation condition or inlet condition.

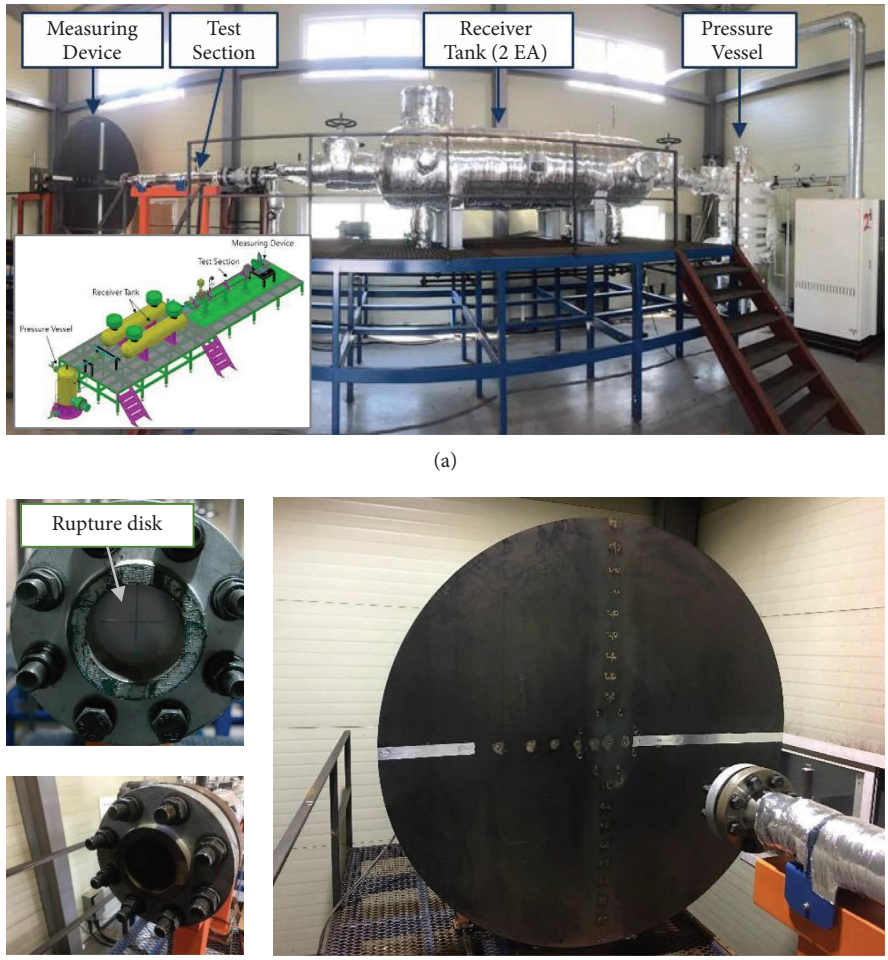

Figure 3: Experimental setup: (a) experimental facilities, (b) test section, and (c) measuring device.

3. Experimental Analysis of the Steam-Jet Impact in the Compartment

3.1. Experimental Equipment and Conditions. A steam-jet collision experiment was performed to yield comparative data for validation of the numerical analysis technique (as reported in existing papers). The experimental equipment consists of a boiler, pressure vessel, electric heater, receiver tank, rupture disk, collision plate, steam pipe, on/off valve, and various measuring equipment (refer to Figure 3). Water preheated through the boiler is transferred to the pressure vessel, and the steam generated by the electric heater installed in the pressure vessel is stored in the pressure vessel and the receiver tank. Moreover, a rupture disk is installed at the end of the steam-injection pipe connected to the receiver tank (refer to Figure 3(a)), and when the internal pressure of the receiver tank attains the target pressure, the valve in front of the rupture disk is opened, thereby rupturing this disk (refer to Figure 3(b)), and the steam jet is sprayed onto the collision plate (refer to Figure 3(c)). The vapor stored in the receiver tank is maintained in a saturated vapor state.

The inner diameter of the pipe in the test section where the steam is injected is 73.7 mm. The steam jet is injected into a disk-shaped impact plate installed with a measuring device, and the diameter of the used impact plate is 2 m with a thickness of 5 mm. During the experiment, the pressure generated by the jet collision was measured by attaching 7 pressure gauges in the radial direction onto the surface of the collision plate.

Experiments were performed according to the initial pressure inside the receiver tank and the jet distance. As the steam jet was injected, the pressure inside the receiver tank decreased, and the internal pressure of the receiver tank at the time the rupture disk was fully opened was employed as the CFD analysis condition. The six experimental conditions used for the CFD analysis are summarized in Table 1, in which the vapor is saturated.

3.2. Verification Analysis Result. CFD analysis was performed using the numerical analysis method under the same conditions as those for the jet-collision experiment performed in the compartment. In addition, the pressure distribution on the collision plate's surface was calculated using the jet model of ANSI/ANS 58.2 for the same conditions. The jet model of ANSI/ANS 58.2 was evaluated by developing a Python-based program in accordance with that reported in the prior state of the art [10].

Table 1: Conditions of the validation analysis for the in-compartment jet-collision test.

Test name	Initial vessel pressure (bar)	Critical mass flux (kg/m^{2}s)	Target distance (mm)	Data time (s)
Jet-A1	20	1493.64	500 (6.78D)	11.884
Jet-A2	20	1445.83	1,000 (13.57D)	11.500
Jet-A3	20	1443.25	1,500 (20.35D)	11.190
Jet-A4	40	1307.70	500 (6.78D)	15.344
Jet-A5	40	1584.61	1,000 (13.57D)	14.586
Jet-A6	40	1584.61	1,500 (20.35D)	15.422

For the verification of the CFD analysis method, the radial pressure distribution of the surface of the collision plate of the experiment, CFD analysis, and the jet model of ANSI/ANS 58.2 were compared with each other. In Figure 4, the X-axis is the radius from the center of the collision plate, and $r/D = 0$ is the center of the collision plate. The Y-axis represents the dimensionless collision pressure based on the upstream pipe pressure (P_0) at the collision plate (equation (8)).

$$P^* = \frac{P(r) - P_\infty}{P_0 - P_\infty}, \tag{8}$$

where P_∞ is the ambient pressure outside the rupture.

Although the pipe upstream pressure (P_0) at the time of evaluation differs for each analysis condition, as the jet-collision distance (L) increases, the jet-collision pressure applied to the center of the collision plate decreases and the collision range tends to increase. The jet model of ANSI/ANS 58.2 underestimates the pressure at the center of the collision plate compared to that in the experiment and predicts a rather wide range of jet influence. In previous studies, the jet model of ANSI/ANS 58.2 oversimplified the structure of the jet [19], overpredicted the expansion of the jet, and underpredicted the distance at which the supersonic effect than the actual jet flow [20]. In addition, it was also found to underestimate the central pressure of the jet at 4.5 D and 6.6 D in the axial distance [17]. Therefore, the CFD analysis result predicted the jet impact pressure distribution more similarly to the verification experiment than the jet model of ANSI/ANS 58.2. The condition simulated in this study is that the collision distance of the jet is 6.78 D–20.35 D, which is remarkably long compared to the inner diameter of the pipe. Accordingly, as reported in previous studies, when the collision distance is extremely short, the collision point pressure is not rendered lower than the jet boundary [13, 14]. If the collision distance is shorter than this experimental condition, the aforementioned phenomenon is expected to occur.

4. Analysis of Steam-Jet Leakage Test in Piping

4.1. Experimental Equipment and Conditions. An experiment was performed on the phenomenon of a small amount of vapor leaking from the pipe, and verification was performed via CFD analysis under the same conditions, and the results were compared. Figure 5 illustrates the test section of the trace-leak steam-jet experimental apparatus. The experimental device consists of a leak-simulation pipe, a steam-supply nozzle, an outer pipe cover, and pressure- and temperature-measuring equipment. Saturated steam with a target pressure of 7 MPa or 10 MPa is sprayed through the nozzle to the outer cover of the pipe, and the inner diameter of the steam-supply nozzle is Ø 1 mm. The outer diameter of the leak-simulation pipe is Ø 88 mm, the inner diameter of the pipe outer cover is Ø 100 mm, and the length of the pipe and the outer cover is 700 mm. The experimental apparatus was configured to adjust the gap between the leaking part and the outer pipe cover, and the experiment was performed by changing the upstream pressure for the cases of 3 and 6 mm. Saturated steam at 7–10 MPa is supplied to the front of the leaking nozzle, and the saturated steam supplied to the outer cover is discharged through the nozzle. To measure the pressure and temperature of the discharged steam, five pressure sensors were installed at an interval of 90 mm from the center of the nozzle to its left and right sides, and four thermocouples were installed 45 mm apart from the pressure sensor to measure the temperature.

4.2. Verification Experimental Equipment and Experimental Conditions. The CFD analysis area is represented by the area between the leak-simulation pipe and the outer cover of the pipe. As the analysis shape is symmetrical, numerical calculations for the 3D analysis domain were performed using a symmetric condition. The upstream conditions measured in the verification experiment and the conditions applied in the CFD analysis are demonstrated in Figure 6 and Table 2. Considering that the center (left side) of the area between the leak-simulation pipe and the outer cover possesses a left–right symmetric shape, a symmetric boundary condition was applied (refer to Figure 6(a)). On the right side of the analysis domain, a pressure boundary condition was applied, and an absolute pressure of 1 atm and a temperature of 25°C were implemented. Insulation conditions were applied to the outer wall of the pipe and the inner wall of the outer cover. Moreover, considering that the shape of the pipe is symmetric when viewed from the side (lateral symmetry), a symmetric boundary condition was applied to the corresponding surface (refer to Figure 6(b)). The gap between the pipe and the outer cover was 3 mm and 6 mm, and the verification analysis was performed under the conditions of 7 MPa and 10 MPa upstream pressure, respectively.

4.3. Results and Discussion. Figure 7 illustrates the jet-collision pressure results corresponding to the steam-jet leaks in the pipe under the condition that the upstream

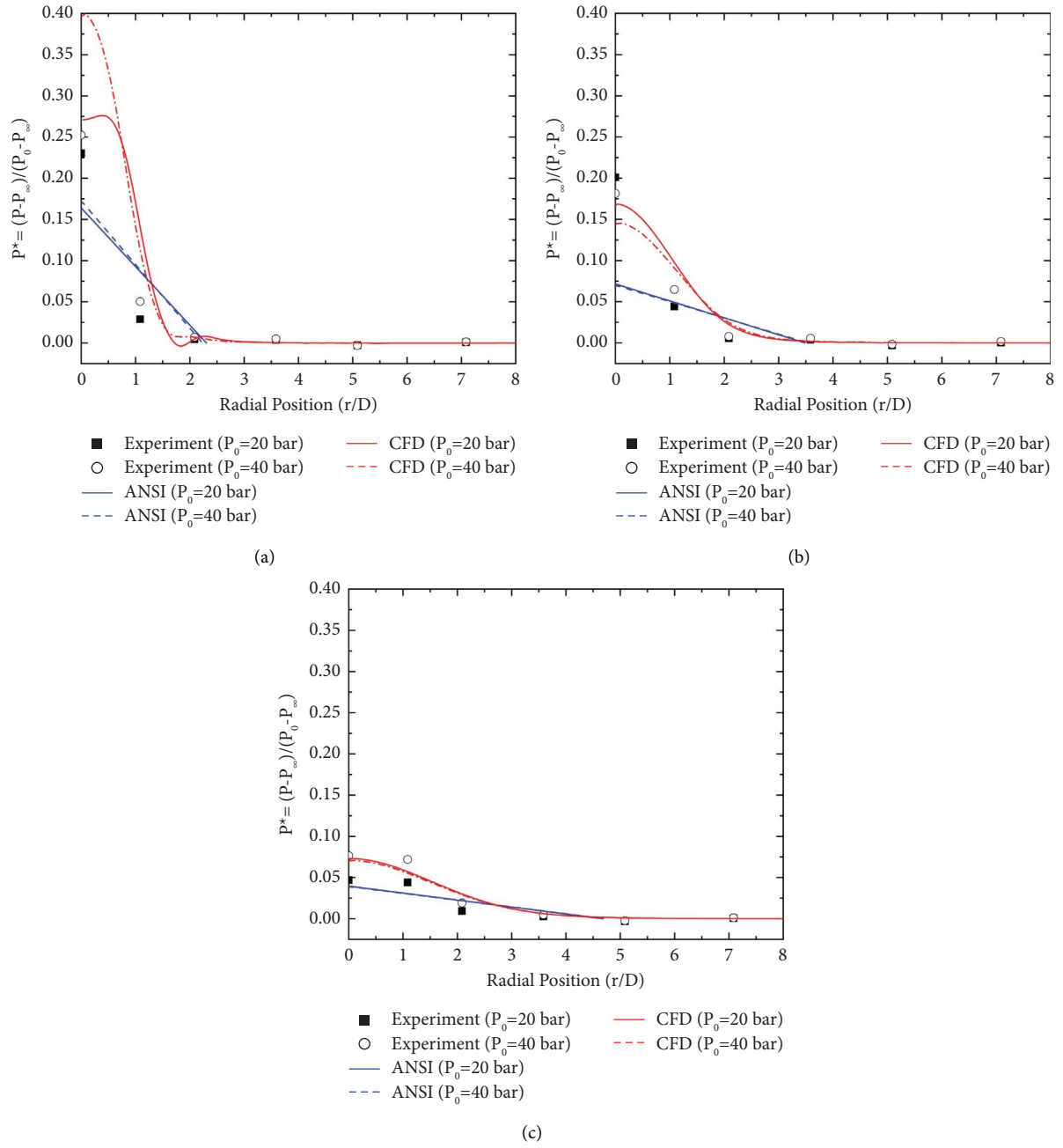

Figure 4: Impinging jet pressure on the target plate: L_{target} = (a) 500 mm (6.78 D), (b) 1000 mm (13.57 D), and (c) 1500 mm (20.35 D).

pressure (P_0) is 7 MPa and 10 MPa. In the analysis, the saturation temperature condition was applied at the upstream pressure condition for the steam. Moreover, the impact pressure of the jet acting on the inner surface of the outer pipe cover was evaluated for each upstream pressure condition, and the pressure evaluated in the experiment was compared with the evaluation result of the jet model obtained via ANSI/ANS 58.2. The characteristics of pressure distribution on the surface point of collision with the jet tend to differ slightly depending on the collision distance of the jet. When the jet impact distance is short ($L/D = 3$) and the upstream pressure is 7 MPa, the pressure is maximal at the center of the impact surface, and a locally high pressure is formed at approximately 2.5 D in the radial direction. This increase in the local pressure is attributed to the effect of compression waves formed at the boundary of the jet [8]. When the upstream pressure is increased to 10 MPa, the impact pressure increases, and as the range of influence of the jet increases, the location of the local-pressure increment tends to increase from 2.5 D to 4 D. In particular, the CFD analysis results and the collision pressure results of the ANSI/ANS 58.2-simulated jet model exhibited similar trends; however, the ANSI model failed to simulate the local-pressure increment at the jet boundary. Notably, in the experiment, the pressure was evaluated at a level approximately 50% lower than that of the CFD analysis. When the

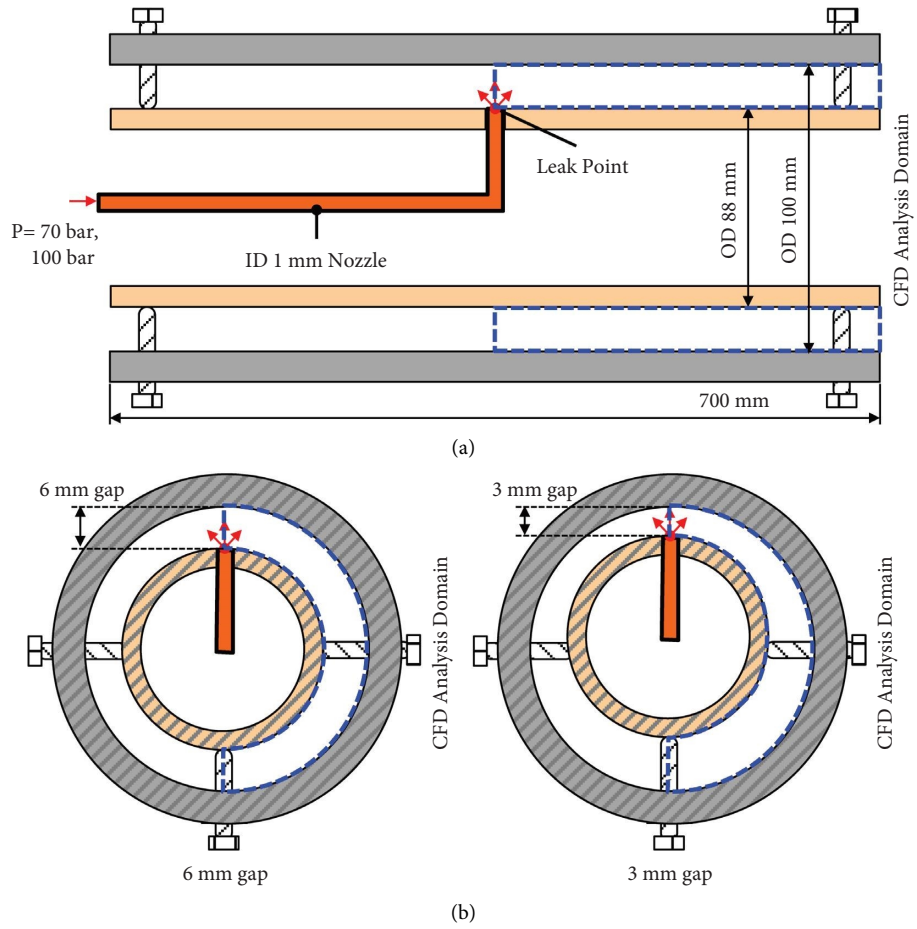

Figure 5: Schematic of the jet experiment: (a) front-view and (b) side-view.

Table 2: Analysis conditions.

		Gap-3 mm-70 bar	Gap-3 mm-100 bar	Gap-6 mm-70 bar	Gap-6 mm-100 bar
Upstream conditions	Pressure (MPa) (PT-B-01)	6.94	9.69	6.82	9.69
	Temperature (°C) (TF-B-01)	277.44	303.27	278.31	300.60
Inlet conditions	Type	Mass flow	Mass flow	Mass flow	Mass flow
	Critical mass flux (kg/m^{2}s)	9890.19	14028.25	9714.05	14028.25
	Quality (-)	1.0	1.0	1.0	1.0
	Hole diameter (mm)	1.0	1.0	1.0	1.0
	Mass flow rate (kg/s) Vapor*	0.0038839	0.0055089	0.0038147	0.0055089
	Throat pressure (MPa)	4.06	5.73	3.99	5.73
	Temperature (°C)	T_{sat}	T_{sat}	T_{sat}	T_{sat}
Boundary conditions	Outlet	Opening, 1 bar, 25°C			
	Pipe outer wall and casing inner wall	Adiabatic wall			

distance between the nozzle and the collision point is proximate to the level of 3 mm, the maximum pressure appears at the center of the jet, and presumably, a particularly low pressure appears because the center is not perfectly aligned with the pressure sensor because of the abnormal behavior of the jet. Even if the center of the steam jet differs slightly by approximately 1-2 mm from the impact point, a large difference can occur in terms of the impact pressure.

When the collision distance of the steam jet is long ($L/D = 6$), the pressure distribution at the center of the collision surface exhibits a flat shape in CFD analysis. In the case of an upstream pressure of 7 MPa, the pressure distribution appears to be higher at the jet boundary than at the center. Presumably, this pressure distribution is because of the formation of a recirculation region between the Mach disk and the collision surface and the formation of an outer jet in

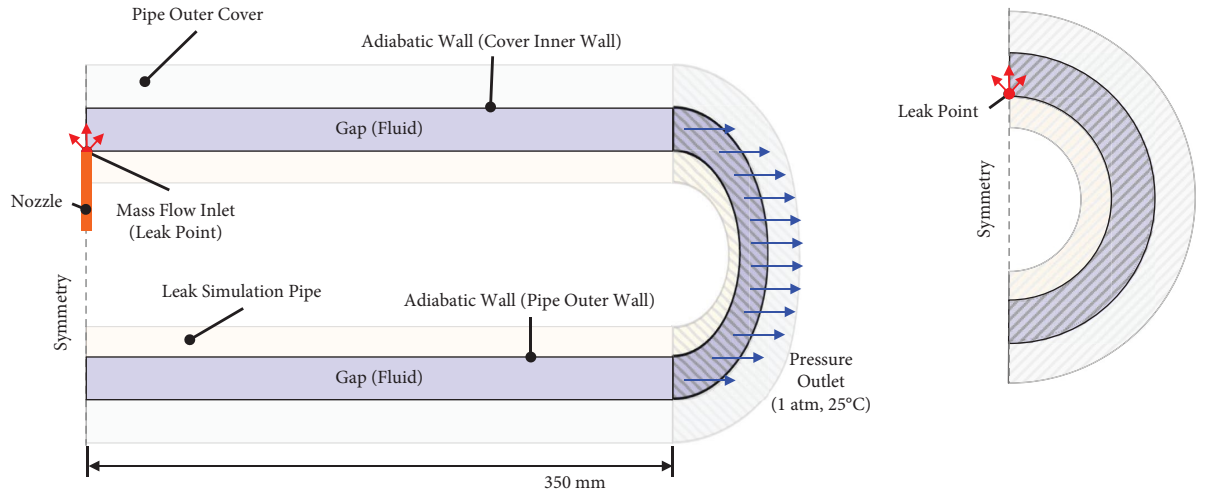

Figure 6: Boundary conditions: (a) front-view and (b) side-view.

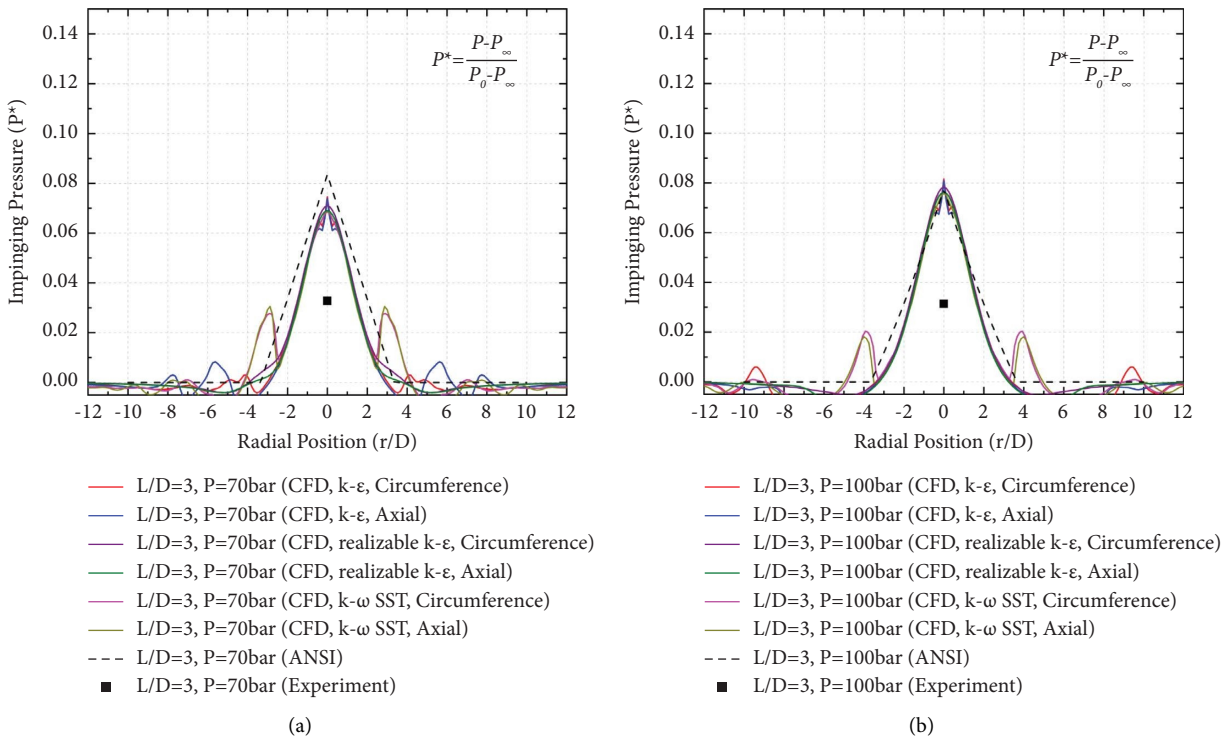

Figure 7: Continued.

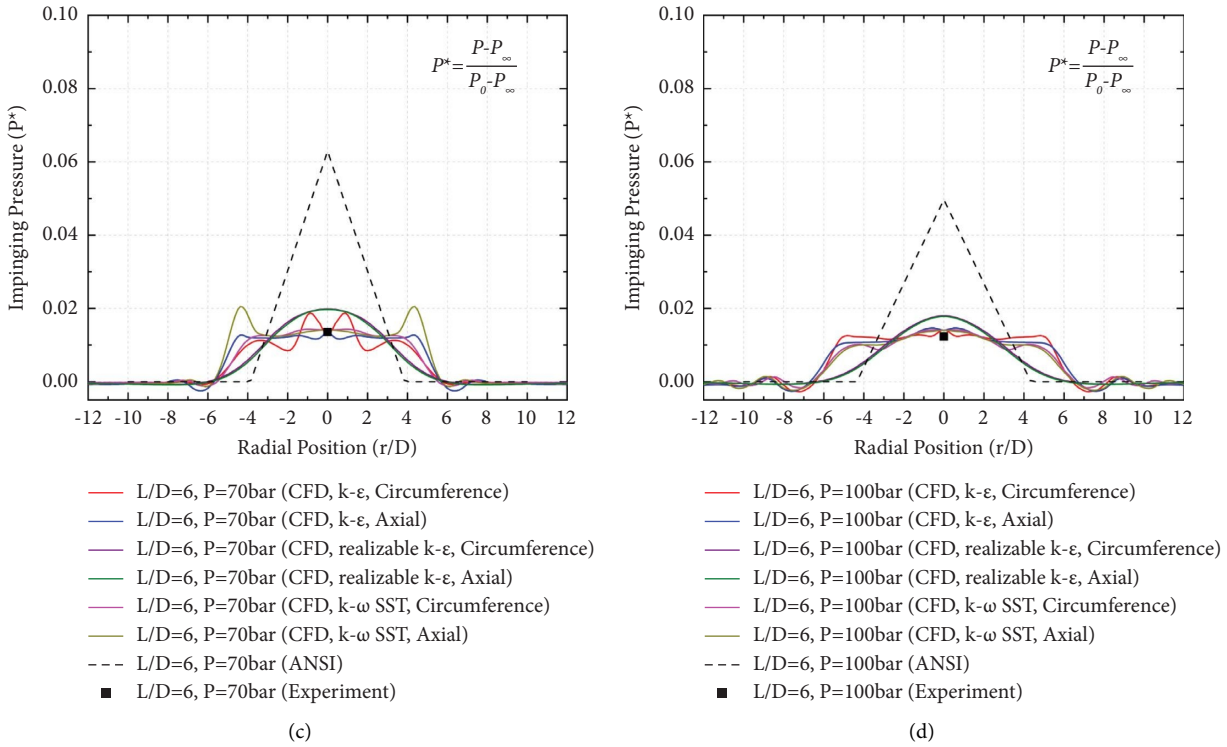

FIGURE 7: Impinging pressure on the inner surface of piping covers: (a) gap 3 mm, $P_0 = 70$ bar, (b) gap 3 mm, $P_0 = 100$ bar, (c) gap 6 mm, $P_0 = 70$ bar, and (d) gap 6 mm, $P_0 = 100$ bar.

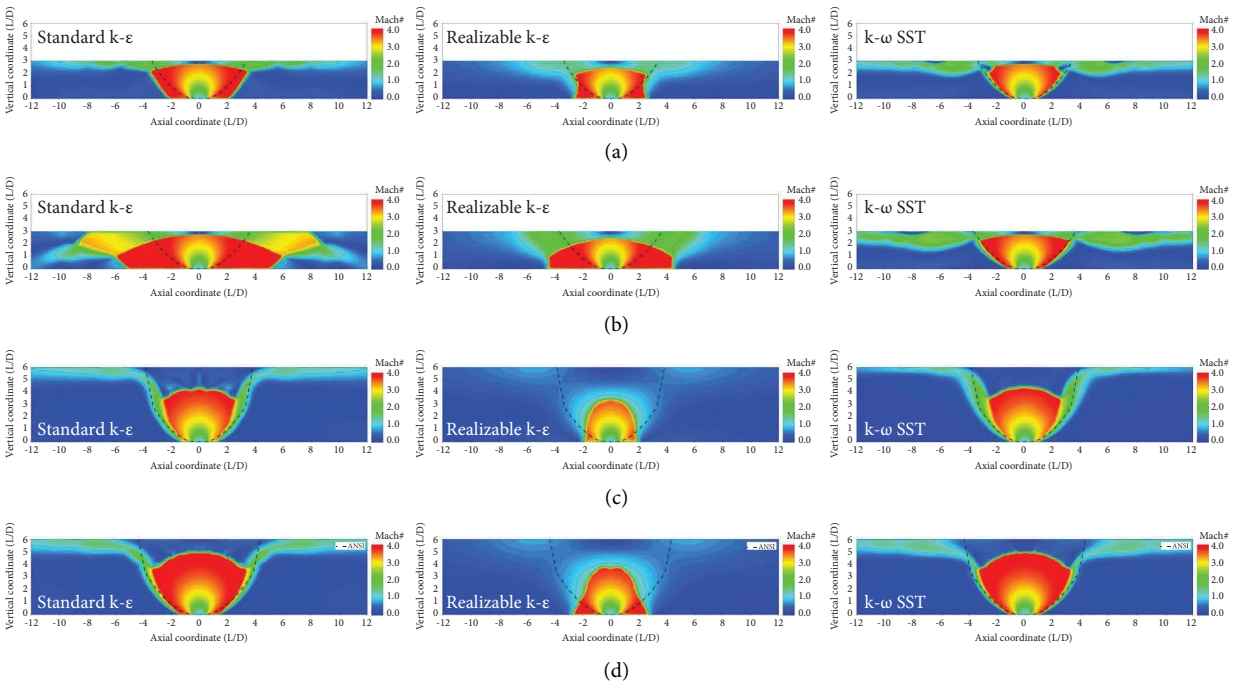

FIGURE 8: Distribution of the Mach number on the front-view: (a) gap 3 mm, $P_0 = 70$ bar, (b) gap 3 mm, $P_0 = 100$ bar, (c) gap 6 mm, $P_0 = 70$ bar, and (d) gap 6 mm, $P_0 = 100$ bar.

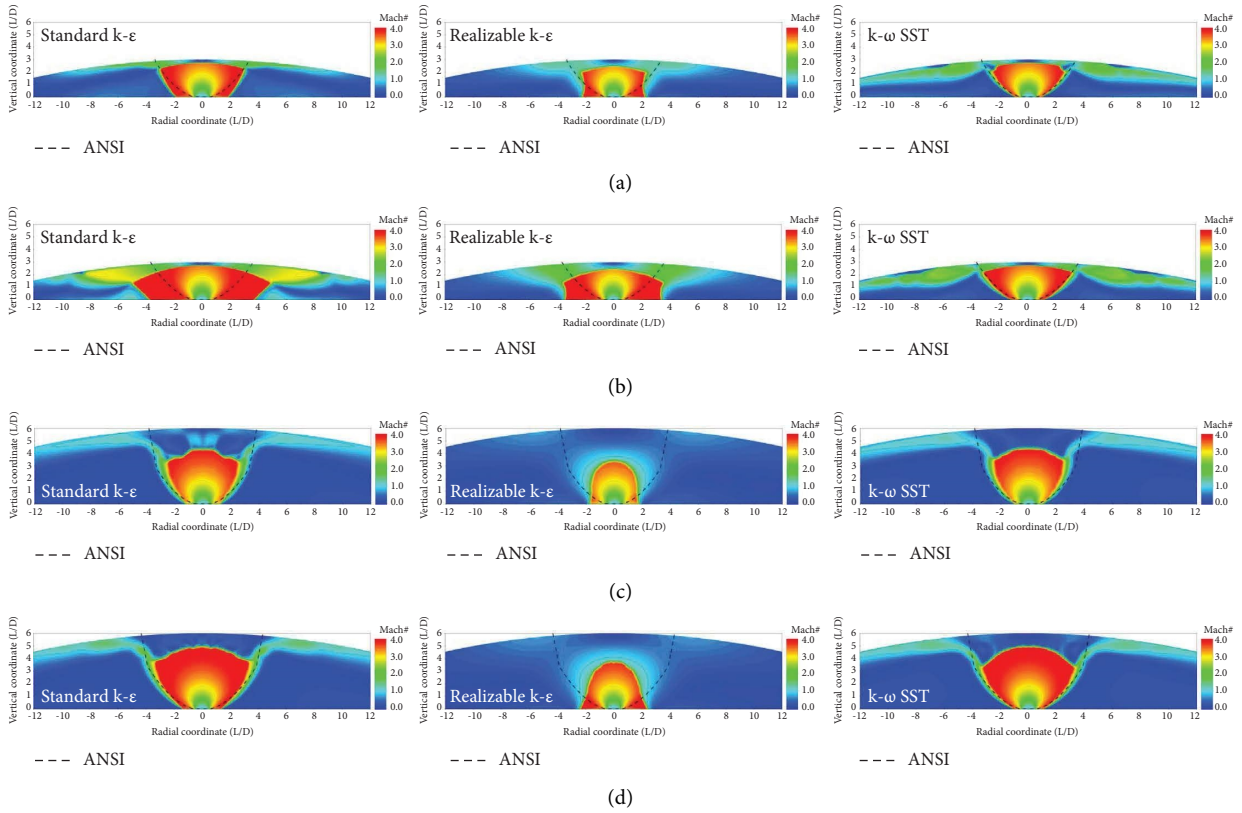

Figure 9: Distribution of the Mach number on the side-view: (a) gap: 3 mm, $P_0 = 70$ bar, (b) gap: 3 mm, $P_0 = 100$ bar, (c) gap: 6 mm, $P_0 = 70$ bar, and (d) gap: 6 mm, $P_0 = 100$ bar.

the boundary region of the jet. Under this condition, the jet model of ANSI/ANS 58.2 predicted the pressure at the center of the collision plate to be larger than that predicted via CFD analysis, evaluating the jet-collision range rather narrowly. In addition, the core pressure results are determined to be at a similar level in the experiment and CFD analysis. Moreover, as a result of the previous study, Oh et al.'s study [14] revealed that, under the condition of the jet-collision distance of 10D or less, the conical subsonic pocket was not formed and the jet spreads in the radial direction. The formation position of the disk tends to move to the upstream side. In this study, the collision distance of the steam jet is less than 6D, and the collision distance was short; thus, the formation position of the Mach disk tends to move upstream as in the previous study.

For the sensitivity analysis of turbulence models, a comparative analysis was performed using the standard k–ε, realizable k–ε, and k–ω SSTs models among the widely used series of RANS-based turbulence models (refer to Figures 7–9). The standard k–ε turbulence model overpredicted the expansion of the steam jet at the leak. Furthermore, the expansion of the steam jet at the leak predicted by the realizable k–ε turbulence model was less than that predicted by the standard k–ε; however, this realizable model could not simulate the flow characteristics of the jet, such as the Mach disk or jet boundary. In contrast, when the k–ω SST turbulence model is applied, the physical phenomena (e.g., Mach disk, barrel shock, and jet boundary) that occur in highly underexpanded jets are well simulated, as shown in Figure 1. In CFD analysis, to simulate the turbulence effect, various turbulence models exist, and differences in the method of evaluating turbulence viscosity depend on the turbulence model. If the analysis was performed under the same conditions, differences in flow characteristics might occur, as shown in Figures 8 and 9. In general, the k–ε model predicts the turbulence characteristics well in the high-speed region, while the SST model is advantageous in predicting the turbulence characteristics in the medium and low-speed regions. Therefore, when the k–ε model was applied in this study, the turbulence effect in the nozzle exit area was well predicted, and the turbulence effect could have been overestimated in the low-speed area relatively far from the nozzle exit. In contrast, using the k–ω SST model, the turbulence effect would be slightly smaller at the nozzle exit; however, it could be appropriately predicted in the area relatively far from the nozzle exit. The k–ω SST model better simulated the characteristics of the highly underexpanded jet than those of other turbulence models (Figures 8 and 9).

On the basis of a comprehensive analysis of the flow characteristics of the steam jet and the pressure distribution characteristics on the surface of the collision point, the CFD analysis was found to afford the behavioral characteristics of the supersonic underexpanded jet in a physically reasonable category. On the contrary, the jet model of ANSI/ANS 58.2

oversimplified the behavior of the steam jet [19], and it was found that the characteristics of a highly underexpanded jet did not appear as in the CFD analysis results.

5. Conclusion

In this study, a numerical analysis method was established to analyze the leakage behavior as the first step in the development of technology for evaluating the trace leakage in the compartment. Subsequently, experimental verification via analysis was performed to validate the established numerical analysis. CFD analysis was performed under the same conditions as the leakage simulation conducted assuming vapor leakage in the compartment and pipe. In the analysis of the vapor-jet collision experiment in the compartment, the jet-collision pressure distribution according to the jet-collision distance yielded results similar to those of the verification experiment. In the analysis of the steam-jet leakage test in the pipe, the flow characteristics of the steam jet and the pressure distribution characteristics on the surface of the collision point were evaluated. A numerical analysis method that could evaluate the behavior characteristics of the supersonic underexpanded jet in a physically reasonable category were established and verified through the sensitivity analysis of the turbulence model. Comparing the numerical analysis performed in this study with the jet model of ANSI/ANS 58.2, in terms of the range of influence (ZOI) and impact pressure, the ANSI/ANS 58.2 jet model oversimplified the behavior of the steam jet, and the changes in local-pressure characteristics in the boundary region and changes in load characteristics at the front/rear end of the Mach disk were not considered. In addition, when the fracture portion and the jet-collision point were located at a sufficient distance from each other, the jet model of ANSI/ANS 58.2 predicted the diffusion angle of the steam jet to be relatively large; thus, the pressure at the center of the jet was found to be lower than the simulation and numerical analysis. Considering the verification and analysis results of the simulation, the numerical analysis method established in this study optimally simulated the compressible flow characteristics of the steam jet, and the numerical analysis results demonstrated a tendency similar to that in the experimental results. In future research, we plan to model a collection system for collecting leaks in a compartment or pipe and conduct a study on performance optimization of the collection system in the event of a leak. The results of this study will aid in comprehending the heat flow characteristics of steam jets formed in the event of a leak in nuclear power plants and will serve as the foundation for the performance evaluation study of the leakage collection system to be performed in the future.

Data Availability

No data were used to support this study.

Conflicts of Interest

The authors declare that they have no conflicts of interest.

Acknowledgments

This work was supported by the Korea Institute of Energy Technology Evaluation and Planning (KETEP), and the Ministry of Trade, Industry, and Energy (MOTIE) of the Republic of Korea (no. 20211510100050).

References

[1] H. S. Jeon, J. S. Suh, G. S. Chae, K. S. Son, S. O. Kim, and N. H. Lee, "Development of leak and vibration monitoring system for high pressure steam pipe by using a camera," *Journal of the Korean Society for Nondestructive Testing*, vol. 36, no. 6, pp. 496–503, 2016.

[2] B. Chexal, J. Horowitz, R. Jones, and B. Dooley, *Flow-accelerated Corrosion in Power Plants. Revision 1*, Electric Power Research Inst, Palo Alto, CA, USA, 1998.

[3] A. Ballesteros, R. Sanda, M. Peinador, B. Zerger, P. Negri, and R. Wenke, "Analysis of events related to cracks and leaks in the reactor coolant pressure boundary," *Nuclear Engineering and Design*, vol. 275, pp. 163–167, 2014.

[4] Korea Institute of Nuclear Safety, "Reports of accident and breakdown in the nuclear power plant," Korea Institute of Nuclear Safety, Daejeon, South Korea, 080606K3, 2008.

[5] Korea Institute of Nuclear Safety, "Reports of accident and breakdown in the nuclear power plant," Korea Institute of Nuclear Safety, Daejeon, South Korea, 170327K4, 2018.

[6] Y. S. Kim, D. J. Euh, W. S. Kim, and T. S. Kwon, "Investigation of leakage characteristics on major equipment/component in reactor system," *The KSFM Journal of Fluid Machinery*, vol. 22, no. 6, pp. 30–35, 2019.

[7] H. Kim and H. Shin, "Numerical study on under-expanded jets through a supersonic Nozzle(II)," *Transactions of the Korean Society of Mechanical Engineers B*, vol. 20, no. 6, pp. 1994–2004, 1994.

[8] J. A. Wilke, P. M. Danehy, R. J. Nowak, and D. W. Alberfert, "Fluorescence imaging study of impinging underexpanded jets," in *Proceedings of the 46th AIAA Aerospace Sciences Meeting and Exhibit*, Reno, NV, USA, January 2008.

[9] A. Krothapalli, Y. Hsia, D. Baganoff, and K. Karamcheti, "The role of screech tones in mixing of an underexpanded rectangular jet," *Journal of Sound and Vibration*, vol. 106, no. 1, pp. 119–143, 1986.

[10] American Nuclear Society, *Design Basis for Protection of Light Water Nuclear Power Plants against the Effects of Postulated Pipe Rupture*, LaGrange, Illinois, IL, USA, 1988.

[11] M. P. Bulat and P. V. Bulat, "Comparison of turbulence models in the calculation of supersonic separated flows," *World Applied Sciences Journal*, vol. 27, no. 10, pp. 1263–1266, 2013.

[12] Ansys Inc, *ANSYS Fluent User Guide (Ver. 18.2)*, ANSYS Inc, Canonsburg, PA, USA, 2017.

[13] J. M. Healzer and E. Elias, "Two-phase jet modeling and data comparison," ERPI, United States, EPRI NP-4362, 1986.

[14] S. Oh, D. K. Choi, W. M. Park, C. Choi, and W. T. Kim, "Development of CFD-based high-energy line break evaluation methodology and its application in the evaluation of supersonic jet impingement load characteristics," *Transactions of the Korean Society of Mechanical Engineers B*, vol. 43, no. 5, pp. 349–359, 2019.

[15] J. J. Jung, W. P. Jang, and D. S. Kim, "A state-of-the-Art report on two-phase critical flow modeling," Korea Atomic Energy Research Institute, KAERI/AR-377/93, 1993.

[16] M. N. Hutcherson, "Contribution to the theory of two-phase blowdown phenomenon," Argonne National Laboratory, Argonne, IL, USA, ANL-75-82, 1975.
[17] S. Kim, M. Ishii, and R. Kong, "Jet impingement in high-energy piping systems, part I: characteristics and model evaluation," *Progress in Nuclear Energy*, vol. 142, 2021.
[18] R. W. Johnson, *The Handbook of Fluid Dynamics*, Springer, Berlin, Germany, 1998.
[19] V. Ransom, *Comments on GSI-191 Models for Debris Generation*, US NRC, Rockville, MD, USA, 2004.
[20] G. Wallis, *The ANSI/ANS Standard 58.2-1988: Two Phase Jet Model*, US NRC, Rockville, MD, USA, 2004.